



Calibration Faint Stars Needs for RVS – II

RVS Calibration

prepared by: C. Allende Prieto
approved by:
reference: GAIA-C6-TN-IAC-CAP-007
issue: 1
revision: 2
date: February 22, 2010
status:

Abstract

Charge Transfer Inefficiency (CTI) in the serial register of the Gaia CCDs distorts significantly the shape of the AC LSF at faint illumination levels, and in particular modifies that shape as a function of the source magnitude and distance from the read-out node. This note makes an evaluation of the level of accuracy in the shape of the AC LSF required for faint RVS sources. This number dictates the fraction of faint observations that need to become calibration faint stars (CFS).

Document History

| Issue | Revision | Date | Author | Comment |
|-------|----------|------------|--------|--|
| 1 | 0 | 2010-02-10 | CAP | Draft |
| 1 | 1 | 2010-02-19 | CAP | Issued after discussing it with Mark Cropper |
| 1 | 2 | 2010-02-22 | CAP | Minor changes suggested by Jos de Bruijne |

Contents

| | | |
|----------|--|----------|
| 1 | Introduction | 5 |
| 2 | Evaluation of impact of AC LSF errors | 5 |
| 3 | Rough estimate | 6 |
| 4 | Numerical simulations | 7 |
| 5 | Conclusions | 9 |
| 6 | Answers to the Action Items #13 and #14 from the GCWG#5 | 9 |

1 Introduction

It has been Noted in CAP-006 that the width of the LSF for the case of a Gaussian can be determined with a precision of about 1% from a single observation of a $G_{\text{RVS}} \sim 8.8$ source, and this uncertainty doubles using a $G_{\text{RVS}} \sim 9.8$ source. The same work estimates that achieving that level of precision for faint stars ($15 < G < 17$) would involve a significant increase in the Gaia telemetry, and therefore a more detailed evaluation of what precision is actually required is in order. This note is devoted to that goal.

2 Evaluation of impact of AC LSF errors

A wrong LSF at faint illumination levels will affect the quality of the data in different ways:

A) It will lead to a wrong evaluation of the signal that may be lost from the window; the error estimates will also be off.

Estimates made by Astrium (see GAIA-EST-MN-10609) indicate that for RVS the maximum loss of signal (when the spectra are read the farthest from the readout node) using the nominal 10-pixel windows are about 5% for a signal of $25 e^-$ and about 20% for a signal of $1.5 e^-$. These losses represent a degradation of the signal-to-noise level of $< 4\%$ and $< 24\%$ for signal levels of 25 and $1.5 e^-$, respectively. Such reductions in signal-to-noise level only impact the accuracy of the derived radial velocities in a modest way. We note that it has been proposed by Astrium that the windows are widened and shifted slightly to reduce the charge loss, although the impact on the number of overlaps (blended spectra) is yet to be determined.

B) It will lead to a wrong evaluation of the expected CTI effects in the serial register, and such errors will be different for absorption lines and in the continuum, due to the lower signal levels around absorption lines.

These effects are expected to be fairly small, as the deepest lines are about 50% of the continuum, and therefore the CTI effects will not be dramatically different. It has also been demonstrated that for the purpose of deriving radial velocities – the sole purpose of the faint RVS spectra ($G_{\text{RVS}} > 14$) – small distortions in the shape of spectral lines have a very limited impact on the precision of the inferred radial velocities (see, e.g., GAIA-C6-SP-MSSL-CAP-004).

C) It will increase the errors involved in processing stars with overlapping windows, i.e. the 'deblending' errors.

As a result of the very low signal-to-noise levels for RVS observations of faint stars, we expect the two first effects above (A and B) to have a limited impact on the derived spectra and radial velocities, and therefore we will focus most of the discussion on 'deblending'.

3 Rough estimate

If all the signal from a star at any given wavelength is within the CCD window, knowledge on the detailed shape of the signal spread in AC is unnecessary. However, when the signal from two neighboring objects overlap, the window will be split and the deblending algorithm will determine how much signal belongs to each source on each of the split windows.

We can approximately evaluate the relative contributions of the error in the signal, and the error in the normalized AC LSF (L), to the signal predicted over a truncated window by considering that the latter is

$$A = N \sum_i w_i L_i, \quad (1)$$

where N is the total signal (electrons) associated with an object (at a given wavelength), and the sum on i is a quadrature over the region in AC included in the relevant window such that $\sum w_i L_i$ approaches unity for a full window. The relative error for the flux in the window is then

$$\sigma^2(A)/A^2 = \frac{(\sum w_i L_i)^2 \sigma^2(N) + N^2 \sum w_i^2 \sigma^2(L_i)}{N^2 (\sum w_i L_i)^2}. \quad (2)$$

In a sense, deblending determines the signal level N from measurements of the signal in the windows, A .

Under the simplifying assumption that the relative errors in the AC LSF are fairly uniform, we define $E \equiv \sigma(L_i)/L_i$, and write for a large-enough window ($\sum w_i L_i \simeq 1$)

$$\sigma^2(A)/A^2 \simeq \sigma^2(N)/N^2 + E^2 \sum w_i^2 L_i^2, \quad (3)$$

which for a Gaussian with a FWHM $\simeq 3$ can be approximated

$$\sigma(A)/A \simeq \sqrt{\sigma^2(N)/N^2 + 0.2E^2}, \quad (4)$$

where $\sigma(N) \simeq \sqrt{N + RON^2}$, and RON is the detector noise, approximately 4 electrons for the case of interest.

Fig. 1 illustrates the shape of the equation above for the cases in which only photon noise is considered (black), only photon noise plus detector noise (red), or when contributions due to errors in the LSF are considered on top of the photon and detector noises (blue for 10% errors and green for 30% errors). At very low signal levels, errors of 30% in the LSF are still quite acceptable.

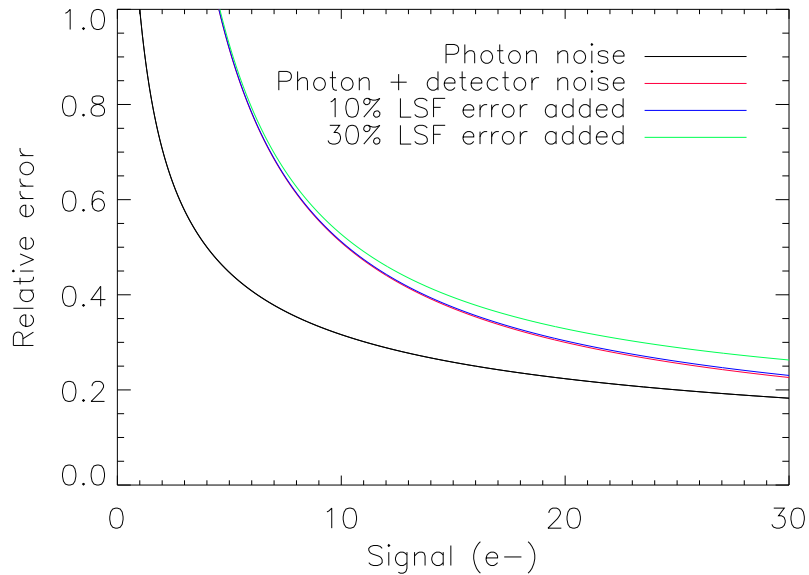


Figure 1: Relative error in the signal in a window recovered from an approximate knowledge of the total signal created by the source and the LSF. The black and red curves correspond to the cases ignoring or considering, respectively, detector noise, but assuming in both that the LSF is known perfectly. The blue and green lines consider errors in the (Gaussian) LSF width of 10 and 30 %, respectively.

4 Numerical simulations

We perform numerical simulations of 2-source blends in order to obtain a better assesment of the impact of errors in the LSF. To simplify, we consider only blends of sources with identical brightness, and separations between 1 and 10 pixels. The AC LSF is assumed to be Gaussian, with a FWHM of 3.0 pixels. We simulate blends considering the photon and the detector noise ($4.0 e^-$ per sample). We run 1000 runs for each combination of source magnitudes and distance and take an average.

We attempt to deblend the sources assuming a perfect knowledge of the width of the LSF. We calculate the mean error and multiply it by a factor 1.25, to estimate the standard deviation, which we compare to the expected noise for isolated sources. The ratio of these two is shown in the top panel of Fig. 2, where we can see that the original signals are properly disentangled for separations larger than 1 *FWHM*, and then errors become significant to reach a three-fold increase at source separations of about 1 pixel.

We then attempt to deblend the sources by adopting an LSF width that is too large by 3%, 10% and 20% (FWHM of 3.1, 3.3 and 3.6 pixels). The ratio of the errors recovered in these test to the

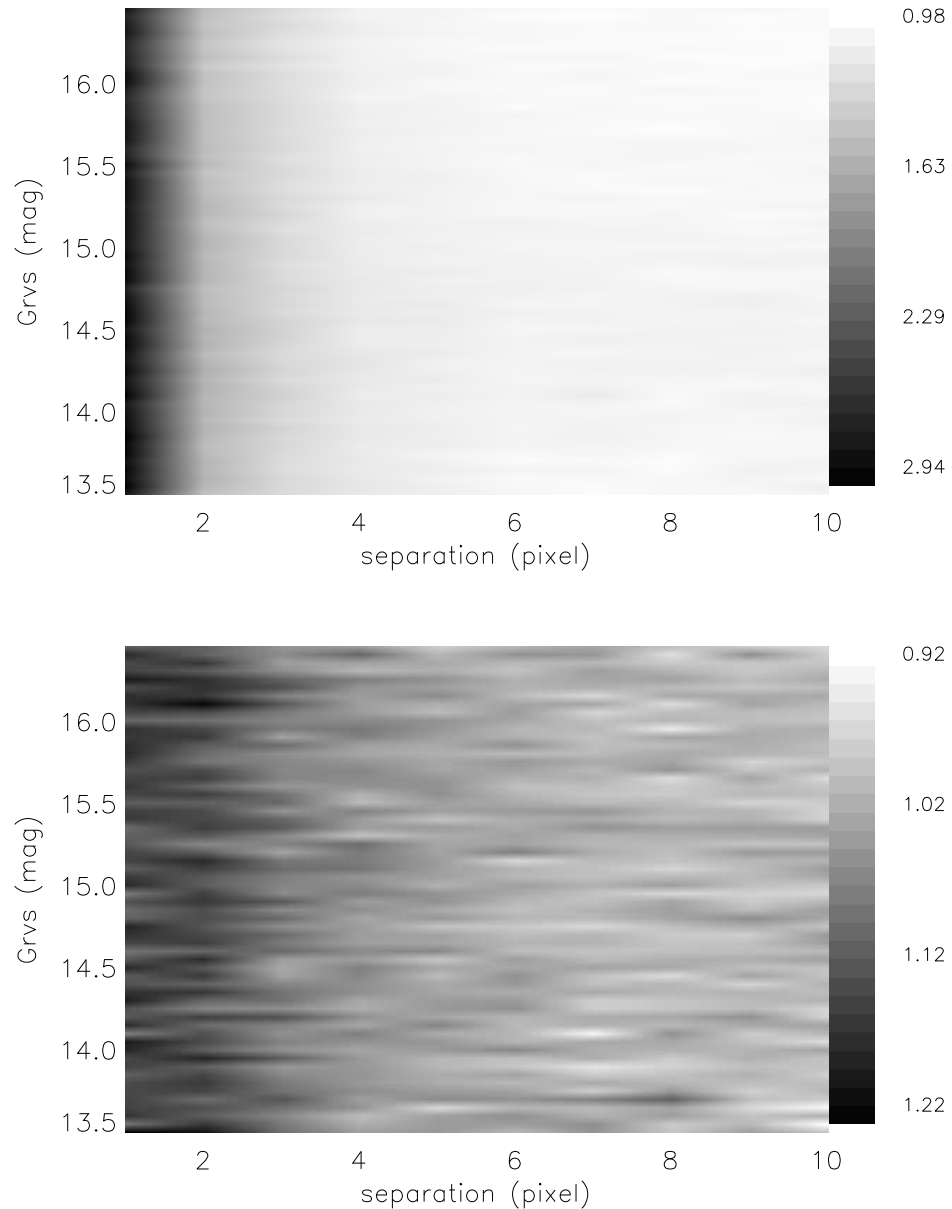


Figure 2: *Top panel:* Ratio of uncertainties in the signal for two deblended identical sources relative to the errors expected for the same sources in isolation. *Bottom panel:* Additional error, on top of that shown in the top panel, caused by an uncertainty of 20% in the width of the LSF.

nominal errors found with the correct LSF width is fairly flat in this limited magnitude range, but the damage is higher at smaller source separations. This ratio is shown in the bottom panel of Fig. 2 for the case of an LSF too wide by 20%. We find maximum increases in the errors of about 10%, 15%, and 20% for errors in the LSF width of 3%, 10% and 20%, respectively.

The magnitudes considered in these tests $13.5 < G_{\text{RVS}} < 16.5$ correspond to signal levels per (AL TDI3) sample of between 0.7 and $10.3 e^-$. In agreement with our previous estimates, errors in the LSF shape do not appear to be very damaging at the faintest magnitudes, and uncertainties of $< 20\%$ in the LSF shape for the faintest RVS sources seem quite tolerable.

5 Conclusions

From the analyses presented here, we find that a knowledge of the AC LSF at the level of $\sim 2\%$, equivalent to the precision attainable by fitting a single CFS for a source with a reference magnitude of $G_{\text{RVS}} = 10$, as discussed in GAIA-C6-SP-MSSL-CAP-006, is not really necessary for the faintest RVS sources ($15 < G < 17$).

We find that adopting a reference magnitude of about $G_{\text{RVS}} \sim 12$ or $G \sim 13$, we can expect errors in the LSF width from CFS observations to be $\sim 10\%$. This will imply having about 0.06% of the observations in the range $15 < G < 17$ as CFS, and an increase in the telemetry of $< 1\%$. We still recommend a fraction of about 0.1 % of the observations in the bin $13 < G < 15$ to become CFS, constraining better the AC LSF shape for sources in this brightness range at a negligible cost in the telemetry.

6 Answers to the Action Items #13 and #14 from the GCWG#5

Based on the conclusions above, these actions are resolved. The proposal for up to 2% of the RVS observations in the range $15 < G < 17$ to be assigned class-0 windows and become CFS is dropped. Instead it is suggested that this fraction be about 0.05-0.06%, which does not involve any significant increase in the telemetry volume. It is also proposed that the fraction of CFS for the range $13 < G < 15$ remain at the $\sim 0.1\%$ level.

With such a reduction in the fraction of CFS at faint magnitudes, the impact on the Gaia performance should remain negligible.